Journal of Biomedical Optics 9(5), 978–981 (September/October 2004)

Optical coherence tomography of malignancy in hamster cheek pouches

Erin S. Matheny
Nevine M. Hanna
W. G. Jung
Zhongping Chen
Petra Wilder-Smith
Beckman Laser Institute
University of California, Irvine
Irvine, California 92612

Reza Mina-Araghi
Matthew Brenner
UC Irvine Medical Center
Pulmonary and Critical Care Division
Orange, California 92868

Abstract. Optical coherence tomography (OCT)/optical Doppler tomography (ODT) provides real-time *in vivo* high-resolution (10-μm) imaging of tissues and real-time spatially resolved blood flow in microvasculature. Hamster cheek pouches with induced dysplasia and malignancies were imaged with OCT/ODT to assess the potential for application to airway malignancy. In 22 Golden Syrian hamsters, 0.5% 9,10-dimethyl-1,2-benzanthracene induces carcinogenesis over 10 weeks in right side cheek pouches; the left side three served as controls. The cheek pouches are imaged *in vivo* prior to sacrifice, and *in vitro* after excision, using a prototype 1310-nm broadband superluminescent diode based OCT/ODT device. Images are compared to standard histopathology. OCT imaging offers good resolution of the hamster cheek pouches to depths of 1 to 3 mm and paralleled histologic images. The feasibility of high-resolution functional imaging is demonstrated in this hamster cheek pouch tumor model. ODT accurately detects vascular change associated with carcinogenesis. [DOI: 10.1117/1.1783897]

Keywords: airway injury; diagnostic; laser; malignant; oral cancer.

Paper 03147 received Dec. 4, 2003; revised manuscript received Jan. 16, 2004; accepted for publication Jan. 16, 2004.

1 Introduction

Technological advances for improving the ability and methods used to assess malignancy and abnormalities in tissues using minimally invasive techniques are important for clinical medicine, particularly for the early diagnosis and localization of carcinoma. Advances in new imaging techniques are improving the range of minimally invasive and noninvasive diagnostic tools available to clinicians.

Optical coherence tomography (OCT) is a new high-resolution optical imaging technique using broadband-limited coherence range laser light that permits minimally invasive imaging of sub-surface abnormalities in complex tissues.[1,2] The engineering principles behind OCT have been described previously.[3] Broadband laser light waves are emitted from a source directed toward a beamsplitter. One beam is sent toward a reference mirror with known path length and the other toward the tissue sample. After the two beams reflect off the reference mirror and surfaces of varying depths within the sample, respectively, the reflected light is directed back toward the beamsplitter where the waves are recombined and read with a photodetector. The image is produced by analyzing the interference patterns of the recombined light waves. Cross-sectional images of tissues are constructed in real-time, at near histologic resolution (10 μm with the current prototype technology used in this study). Once optimized, OCT may provide the capability of obtaining noninvasive high-resolution optical images of superficial tissues using flexible fiberoptic probes for a range of medical applications.[1]

OCT imaging has been compared to ultrasound scanning conceptually.[4] Both techniques provide structural imaging. However, unlike ultrasound, which utilizes sound waves, OCT takes advantage of the short coherence length of broadband laser light reflection interference to create very high-resolution images.[4] OCT uses the backscattering of light from tissue components of differing refractive indicies to create the 2-D gray-scale images. Even though clinical OCT technology is still in the early developmental stages, 10-μm-resolution images can be obtained with relatively inexpensive superluminescent diode laser source systems. This imaging technology has been demonstrated to have potential clinical applications in dermatology,[5,6] ophthalmology,[7,8] and cardiology.[9]

Another important evolving aspect of OCT technology is optical Doppler tomography (ODT). ODT enables noninvasive spatially localized imaging of tumor neovasculature and monitoring of changes in blood flow.[10]

The purpose of this study was to determine the ability of OCT imaging to detect and diagnose histologic changes associated with oral dysplasia and malignancy. The Golden Syrian hamster (*Mesocricetus auratus*) cheek pouch model was used. This model of oral malignancy is well established for upper airway tumor induction. Hamster cheek pouch dysplasia and squamous cell carcinoma are comparable histologically to those in the human oral cavity.[11,12] Dysplasia and tumors were induced in hamster cheek pouches and imaged *in vivo* and *ex vivo* at varying stages of carcinogenesis—from healthy, through dysplasia, to squamous cell carcinoma. OCT images were compared with conventional histological sections to determine the ability of OCT to detect upper airway premalignancies and malignancies, and also to map changes in indi-

Address all correspondence to Matthew Brenner, UC Irvine Medical Center, Pulmonary and Critical Care Division, Bldg. 53, Rm. 119, 101 City Drive South, Orange, CA 92868. Tel: 714-456-5150; Fax: 714-456-8349; E-mail: mbrenner@uci.edu

1083-3668/2004/$15.00 © 2004 SPIE

vidual blood vessel morphology throughout carcinogenesis. ODT identified changes in blood volume and velocity during the process of carcinogenesis were assessed.

2 Materials and Methods

2.1 *Tumor Induction*

Hamsters were divided into three groups for the study: control animals ($n=2$), *ex vivo* excised imaging ($n=6$), and *in vivo* imaging ($n=16$). The standard Golden Syrian hamster (*Mesocricetus auratus*) cheek pouch model was used.[11,12] Half a percent (0.5%) DMBA (9,10 dimethyl-1,2-benzanthracene) was applied thrice weekly to the right cheek pouch in 22 hamsters for weeks 0 to 16. In the control left cheek pouch of these hamsters and in both pouches of additional control hamsters, only mineral oil was applied. This design enabled OCT and histological evaluation of DMBA-untreated healthy cheek pouches. Previous studies have demonstrated that the carcinogenesis process in one cheek pouch does not affect the other cheek pouch,[11,12] and therefore that the untreated cheek pouch can be used as control. Dysplasia developed in DMBA-treated cheek pouches in approx. 4 to 6 weeks, progressing to squamous cell carcinoma after approximately 8 to 16 weeks. The animals were treated in accordance with Animal Resources Center (ARC) guidelines at the University of California at Irvine[12] (UCI) (IACUC 97-1972).

2.2 *Animal Handling*

The hamsters were placed in a chamber and inhalational anesthesia was administered. One half of the control group as well as the excised imaged group hamsters were euthanized and their cheek pouches were removed and imaged.

Half of the control group and the *in vivo* imaged animals were then anesthetized further with intraperitoneal 2:1 ketamine HCL (100 mg/ml): xylazine (20 mg/ml) at a dose of 0.75 cm^3/kg using a 25-gauge needle. These animals were then wrapped in Mylar to prevent hypothermia. The cheek pouches were inverted, held in place with a fixation device, and imaged. After the imaging, the hamsters were euthanized and the specimens were excised for histologic preparation.

2.3 *Imaging*

In the excised model animals, the cheek pouches were immediately excised after sacrifice and prepared for OCT/ODT imaging. The tissue section was stretched over cork and pinned using 0.20-mm insect pins. The cheek pouches were then covered with a thin layer of KY Gel to prevent the desiccation of the tissue during the imaging process (Johnson & Johnson Product Inc., New Jersey). Triangular shaped notches were cut at opposite ends of the tissue to document a line of image acquisition. A visible He-Ne laser guide beam was used to position the samples for OCT/ODT acquisition on the stage. After imaging, the tissue was placed in formalin, fixed, and prepared for standard paraffin sections, H&E (hematoxylin and eosin) staining and histological evaluations. For the *in vivo* studies, the cheek pouches were everted and imaged. Pins were used to mark the line of image acquisition. After the animal was sacrificed, the tissue was harvested and prepared for standard paraffin sections H&E staining and histological evaluation.

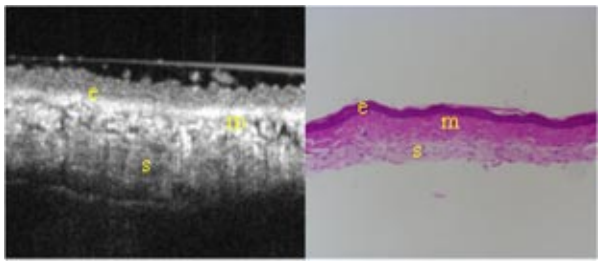

Fig. 1 OCT image (left) of a normal hamster cheek pouch versus H&E stained histological section (right): e, squamous epithelum; m, mucosa; s, submucosa.

The OCT/ODT images for each tissue sample were compared alongside the histology section using an Olympus BH2 light microscope (with a 4 and 6.3 objective lens). Areas of the histology section corresponding to the OCT/ODT images were then photographed using an Olympus DP10 camera for a light microscope and Olympus Digital Vision 3.1 computer program. The histological images were aligned with the corresponding OCT and ODT images.

2.4 *Histological Evaluation*

Histological evaluation of each stained section was quantified by two blinded, prestandardized scorers (one oral pathologist, one dentist). Each characteristic listed here was assessed. The following numerical grading system was used for each slide: 0, healthy; 1, hyperkeratosis; 2, mild dysplasia; 3, moderate dysplasia; 4, severe dysplasia; 5, carcinoma in-situ; and 6, squamous cell carcinoma (SCC). The criteria for oral epithelial dysplasia were as follows: drop-shaped rete ridges, irregular epithelial stratification, individual cell keratinization, basal cell hyperplasia, loss of intercellular adherence, loss of polarity, hyperchromatic nuclei, increased nucleocytoplasmic ratio, anisocytosis, pleomorphic cells and nuclei, abnormal mitotic figures, and increased mitotic activity. Each site was assessed for each of these characteristics at a level of either none (0), slight (1), or marked (2).

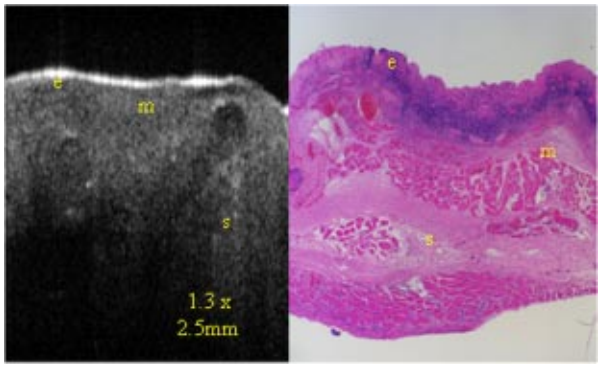

Fig. 2 *In vivo* OCT image (left) of cheek pouch with dysplasia versus the histological section (right). Epithelial thickening, inflammation and increased cellular proliferation are evident: e, squamous epithelum; m, mucosa; s, submucosa.

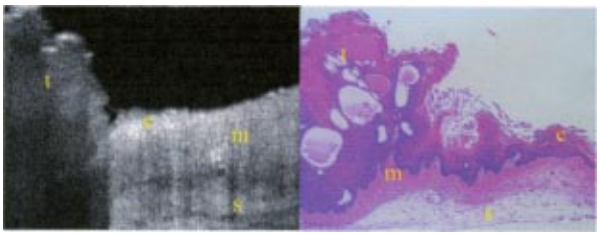

Fig. 3 OCT image (left) of squamous cell carcinoma in a malignant hamster cheek pouch. The corresponding histological section (right) shows analogous location H&E image: e, squamous epithelium; m, mucosa; s, submucosa; t, fungiform malignant tissue; b, basement membrane.

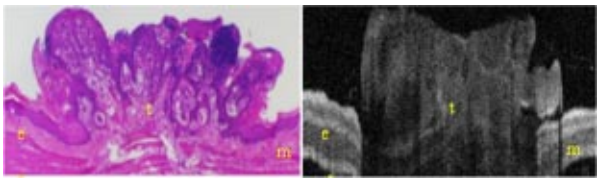

Fig. 4 Histology (left) versus OCT image of hamster cheek pouch containing squamous cell carcinoma tumor: e, squamous epithelium; m, mucosa; s, submucosa; t, fungiform malignant tissue; b, basement membrane.

2.5 *OCT Evaluation*

The two pretrained scorers classified each image diagnostically in a blind manner on a scale of 0 (normal) to 6 (SCC). This scale was designed to parallel the scale used for histopathological evaluation. OCT diagnostic scores were based on changes in keratinization, epithelial thickening, epithelial proliferation and invasion, broadening of rete pegs, irregular epithelial stratification, and basal hyperplasia. Epithelial invasion was defined as loss of visible basement membrane. Each site was assessed for each of the above characteristics at a level of either none (0), slight (1), or marked (2). The score for each site depending on the range and severity of individual features and the proportion of epithelial thickness affected.

Data consisted of descriptive images. Each scorer evaluated all data in one session, which took place once all data accrual was complete. A second reevaluation of all images by the same scorers in one session 3 to 4 months later was used to evaluate intraobserver variability.

3 Results

Images obtained using optical coherence tomography were very similar to the corresponding histological sections in all cases (Figs. 1–4). Normal hamster cheek pouches imaged using OCT demonstrate the near-histologic level imaging capabilities of OCT. Tissue layers are detectable using OCT imaging techniques, as illustrated in Fig. 1. The comparison between normal hamster cheek pouch histology and OCT images reveal the intact squamous epithelium, mucosal, and submucosal layers within the tissue.

Images taken from the left cheek pouches were used for control and did not show any sign of dysplasia or malignancy. The right cheek pouches demonstrated varying degrees of architectural changes with varying degrees of dysplasia and squamous cell carcinoma.

In vivo image (Fig. 2) illustrates the ability of OCT to detect dysplasia and epithelial changes associated with it. Epithelial thickening into the underlying connective tissue is evident. Further advancement into squamous cell carcinoma of the hamster cheek pouch is displayed in Fig. 3, with its corresponding histological image.

OCT images containing tumors appear to have more scattering and absorptive regions compared to normal tissue, reducing overall depth of penetration of images. The tumor and histological images in Fig. 4 comparing squamous cell carcinoma in a fungiform malignant tumor reveal that the epithelium is folded, as is the mucosa and basement membrane. The basement membrane is no longer intact due to the invasion of the malignant cells into the connective tissue below.

Figure 5 shows *in vivo* images of progressive changes throughout carcinogenesis in morphology and perfusion of one specific blood vessel in a hamster cheek pouch. Over time, blood vessel size, blood volume, and flow velocity increased with progressive dysplasia, especially from 7 weeks carcinogenesis onward. In the adjacent tissues, epithelial and subepithelial proliferative changes were visible.

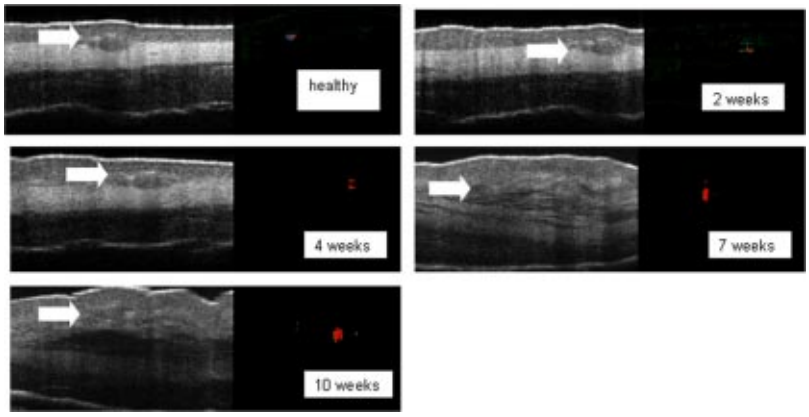

Fig. 5 *In vivo* OCT (left-hand-side) and ODT (right-hand-side) images of hamster cheek pouch mucosa in the same animal throughout carcinogenesis. OCT images show progressive epithelial and subepithelial change and blood vessels (arrow). ODT images show increased velocity and volume of blood flow (color-coded in red as to show the blood flow).

4 Discussion

Recently developed OCT technology enables minimally invasive imaging of complex tissues to a depth of 1 to 3 mm, with very high (10-μm) resolution.[2,13,14] This enables OCT to be adapted for a wide variety of clinical applications, with potential for *in vivo* detection and localization of dysplasia and malignancy in the upper and lower airways and pleura. Future advances in OCT resolution to near cellular level may further enhance the clinical usefulness of this modality. Even at current resolution limits, the ability to detect epithelial and subepithelial changes in the hamster cheek pouches demonstrates the diagnostic potential of OCT, in this example, for differentiating between dysplasia and malignancy. At current levels of resolution, OCT may aid in selecting biopsy locations, or in the detection of submucosal abnormalities that may be difficult to visualize and identify correctly from the surface. The ability of OCT to image individual blood vessels consistently and determine accurate spatially resolved flow velocities lends itself well to research applications. Particularly relevant areas are in carcinogenesis investigations, where the time-based and spatially based interaction between tissue and vascular factors controlling angiogenesis remains unresolved.

ODT images obtained in these study animals demonstrated localized microvascular blood flow increases throughout carcinogenesis. Little vascular change was seen in early stages of premalignant change. However, at 7 weeks (moderate to severe dysplasia), and even more so at 10 weeks (carcinogenesis and severe dysplasia), considerable increases in blood volume and flow were apparent.

OCT/ODT is a promising high-resolution imaging technology in the early stages of clinical development. OCT offers high-resolution real-time imaging of the hamster cheek pouches including the ability to detect malignancy and fine detail in tissue in both *in vivo* and *in vitro* conditions. OCT has the capability to be adapted into flexible fiber optic probes to be used *in vivo*. A portable fiber optic OCT device with the ability to obtain real-time, high-resolution images has numerous potential clinical applications. Additional studies are currently underway to improve image resolution, acquisition time, and probe designs.

Acknowledgments

We would like to thank Tanya Burney, Teri Waite-Kennedy, Tatiana Krasieva, and David Mukai for their technical assistance with this study. This research is supported by Tobacco-Related Disease Research Program (TRDRP) Grant No. 9RT-0094; Air Force Grant No. F49620-00-10371; National Institutes of Health (NIH) Grant No. EB-00293; National Cancer Institute (NCI) Grant Nos. 91717 and RR-01192.

References

1. J. A. Izatt, M. D. Kulkami, K. Kobayashi, M. V. Sivak, J. K. Barton, and A. J. Welch, ''Optical coherence tomography for biodiagnostics,'' *Opt. Photonics News* **8**, 42–47 (1997).
2. D. Zhihua, R. Hongwu, Z. Yonghua, J. S. Nelson, and C. Zhongping, ''High-resolution optical coherence tomography over a large depth range with an axicon lens,'' *Opt. Lett.* **27**, 243–245 (2002).
3. B. E. Bouma and G. J. Tearney, *Handbook of Optical Coherence*, Marcel Dekker, New York (2002).
4. P. J. Tadrous, ''Methods for imaging the structure and function of living tissues and cells: 3. Confocal microscopy and microradiology,'' *J. Pathol.* **191**, 345–354 (2000).
5. B. H. Park, C. Saxer, S. M. Srinivas, J. S. Nelson, and J. F. de Boer, ''In vivo burn depth determination by high-speed fiber-based polarization sensitive optical coherence tomography,'' *J. Biomed. Opt.* **6**, 474–479 (2001).
6. N. D. Gladkova, G. A. Petrova, N. K. Nikulin, S. G. Radenska-Lopovok, L. B. Snopova, Y. P. Chumakov, V. A. Nasonova, V. M. Gelikonov, G. V. Gelikonov, R. V. Kuranov, A. M. Sergeev, and F. I. Feldchtein, ''In vivo optical coherence tomography imaging of human skin: norm and pathology,'' *Skin Res. Technol.* **6**, 6–16 (2000).
7. G. J. Tearney, I. K. Jang, D. H. Kang, H. T. Aretz, S. L. Houser, T. J. Brady, K. Schlendorf, M. Shishkov, and B. E. Bouma, ''Porcine coronary imaging in vivo by optical coherence tomography,'' *Acta Cardiol.* **55**, 233–237 (2000).
8. J. Ge, R. Luo, and Y. Guo, ''Corrective change of retinal thickness measured by optical coherence tomography and histologic studies,'' *Yan Ke Xue Bao* **15**, 153–155, 178 (1999).
9. T. M. Yelbuz, M. A. Choma, L. Thrane, M. L. Kirby, and J. A. Izatt, ''Optical coherence tomography: a new high-resolution imaging technology to study cardiac development in chick embryos,'' *Circulation* **106**, 2771–2774 (2002).
10. R. E. Reiss, ''Umbilical artery Doppler velocimetry: applications and limitations,'' *Am. J. Perinatol* **8**, 293 (1991).
11. S. Charoenbanpachon, T. Krasieva, A. Ebihara, K. Osann, and P. Wilder-Smith, ''Acceleration of ALA-induced PpIX fluorescence development in the oral mucosa,'' *Lasers Surg. Med.* **32**, 185–188 (2003).
12. A. Ebihara, T. B. Krasieva, L. H. Liaw, S. Fago, D. Messadi, K. Osann, and P. Wilder-Smith, ''Detection and diagnosis of oral cancer by light-induced fluorescence,'' *Lasers Surg. Med.* **32**, 17–24 (2003).
13. G. J. Tearney, M. E. Brezinski, B. E. Bouma, S. A. Boppart, C. Pitris, J. F. Southern, and J. G. Fujimoto, ''In vivo endoscopic optical biopsy with optical coherence tomography,'' *Science* **276**, 2037–2039 (1997).
14. P. J. Tadrous, ''Methods for imaging the structure and function of living tissues and cells: 1. Optical coherence tomography,'' *J. Pathol.* **191**, 115–119 (2000).